Optical properties and molecular orientation in organic thin films

2003 J. Phys.: Condens. Matter 15 S2699

(http://iopscience.iop.org/0953-8984/15/38/009)

INSTITUTE OF PHYSICS PUBLISHING JOURNAL OF PHYSICS: CONDENSED MATTER

J. Phys.: Condens. Matter **15** (2003) S2699–S2718 PII: S0953-8984(03)67377-7

Optical properties and molecular orientation in organic thin films

M Friedrich[1,4], G Gavrila[1], C Himcinschi[1], T U Kampen[1], A Yu Kobitski[1], H Méndez[1], G Salvan[1], I Cerrilló[2], J Méndez[3], N Nicoara[2], A M Baró[2] and D R T Zahn[1]

[1] Institut für Physik, Technische Universität Chemnitz, D-09107 Chemnitz, Germany
[2] Laboratorio de Nuevas Microscopías, Departamento Física de la Materia Condensada, Universidad Autónoma de Madrid, E-28049, Spain
[3] Instituto de Ciencia de Materiales de Madrid, CSIC, E-28049, Spain

E-mail: friedrich@physik.tu-chemnitz.de

Received 6 August 2003
Published 12 September 2003
Online at stacks.iop.org/JPhysCM/15/S2699

Abstract

The optical properties and the molecular orientation in thin films of 3,4,9,10-perylenetetracarboxylic dianhydride (PTCDA) and N,N'-dimethyl-3,4,9,10-perylenetetracarboxylic diimide (DiMePTCDI) were studied by means of variable angle spectroscopic ellipsometry (VASE), atomic force microscopy (AFM), near edge x-ray absorption fine structure (NEXAFS) spectroscopy, and infrared (IR) and Raman spectroscopy. VASE reveals that both kinds of film exhibit a strong optical anisotropy. For PTCDA, the optical constants are found to have much higher values in the substrate plane than perpendicular to it. While the anisotropy measured in the substrate plane on passivated GaAs(100) is very small for PTCDA a giant anisotropy is observed for DiMePTCDI. This difference in the optical properties is attributed to the different orientation of molecules in the thin organic films. While the PTCDA molecules lie flat on the substrate with their molecular plane parallel to the substrate surface, the DiMePTCDI molecules are tilted with respect to the substrate surface and are predominantly oriented with their long axis parallel to the [011] direction of the substrate as confirmed by VASE, NEXAFS, and Raman and IR results.

1. Introduction

Perylene derivatives are commercially available red pigments with electrical and optical properties that allow them to be compared to conventional inorganic wide band gap semiconductors.

[4] Author to whom any correspondence should be addressed.

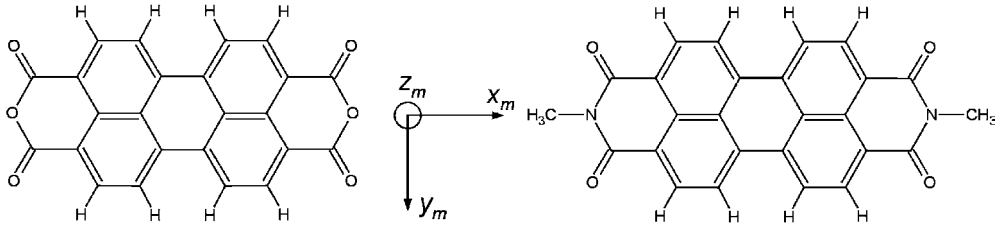

Figure 1. The chemical structure of PTCDA and DiMePTCDI molecules.

Table 1. Unit cell parameters for PTCDA and DiMePTCDI. The angle φ_u describes the angle between the long molecular axis and the *b* direction of the unit cell (see figure 13).

Parameter	α-PTCDA[a]	β-PTCDA[a]	DiMePTCDI[b]
Space group	$P2_1/c$ (C^5_{2h})	$P2_1/c$ (C^5_{2h})	$P2_1/c$ (C^5_{2h})
a (Å)	3.74	3.78	3.87
b (Å)	11.96	19.30	15.58
c (Å)	17.34	10.77	14.60
β (deg)	98.8	83.6	97.65
Z	2	2	2
φ_u (deg)	42	52	18

[a] From [1].
[b] From [4].

The asymmetry in the structure of molecular crystals and thin films gives rise to anisotropic physical properties. In 3,4,9,10-perylenetetracarboxylic dianhydride (PTCDA) films, for instance, the conductivity is extremely anisotropic, with the in-plane conductivity being lower by at least six orders of magnitude compared to that perpendicular to the plane [1]. Zang *et al* [2] and Friedrich *et al* [3] demonstrated the anisotropic optical properties of thin PTCDA films and the pronounced differences for in- and out-of-plane optical constants. The electronic and optical characteristics of individual molecules are dominated by their structure which can be modified by molecular tailoring. The colour of these materials in the solid state is additionally influenced by the crystalline structure. Hädicke *et al* [4–6] reported the solid-state effect of crystallochromy for N,N'-substituted-3,4,9,10-perylenetetracarboxylic diimide (R-PTCDI) with different peripheral R-groups such as methyl or butyl. The absorption spectra corresponding to π–π^* transitions of R-PTCDI in the crystalline state shift depending on the electronic interaction between the close-packed perylene planes. The interaction can be varied by different steric effects of the substituted R-groups.

Amongst the perylene derivatives PTCDA is considered to be an archetype molecule. PTCDA has a planar rectangular geometry consisting of a perylene core terminated by oxygen atoms in the dianhydride form as can be seen in figure 1. Considering thin film growth of these molecules several groups found two polymorphs called α and β [7, 8]. Both crystallize in the space group $P2_1/c$ but have different lattice constants as summarized in table 1. The unit cell contains two molecules which are arranged in a herringbone packing with the molecular planes parallel to the (102) lattice plane. In the α modification the overlap between molecules in adjacent (102) crystalline planes is reduced by shifting along the short unit cell axis, while the reduction for the β phase occurs via shifting along the long axis. On clean InAs(001) substrates the first monolayer PTCDA interacts strongly with the substrate and two-dimensional overlayers are formed [9]. For larger coverages a phase transition occurs where bulk-like

three-dimensional PTCDA clusters begin to form. The strong interaction between PTCDA and semiconductor surfaces is considerably reduced by a passivation of the surface prior to the growth of the organic film [10, 11]. Indeed, improved crystallinity is observed for depositions on sulfur passivated GaAs(100) [12, 13].

N,N'-dimethyl-3,4,9,10-perylenetetracarboxylic diimide (DiMePTCDI) has a planar perylene core with four carboxylic and two imide groups terminated by two three-dimensional CH_3 groups as sketched in figure 1. DiMePTCDI crystallizes in the same monoclinic structure as PTCDA. The unit cell parameters are given in table 1.

Various tilt angles for the molecular orientation are reported in the literature dependent on the substrate used. In thick films (300 nm) of DiMePTCDI grown on glass substrates most of the molecules are parallel to the substrate, some of them being tilted with a Gaussian distribution with FWHM of 22° [14]. Similarly it was found that the molecules on KCl(100) substrates lie close to parallel with the substrate plane [15]. A large tilt ($\theta = 90°$) was observed by means of LEED and STM for monolayer films of DiMePTCDI on Ag(110) substrates [16] where a pronounced in-plane optical anisotropy was also detected [17]. Even on the same substrate, e.g. Ag(110), various orientations can coexist [18].

In this work the optical properties of thin PTCDA and DiMePTCDI films are investigated by variable angle spectroscopic ellipsometry (VASE). Furthermore, the orientation of DiMePTCDI molecules on passivated GaAs(100) surfaces is investigated by atomic force microscopy (AFM), near edge x-ray absorption fine structure (NEXAFS) spectroscopy, as well as Raman and IR spectroscopy and compared to the orientation of the archetype molecule PTCDA.

2. Experimental details

Samples were prepared under ultrahigh vacuum (UHV) conditions on passivated GaAs(100) and for comparison on Si(111) surfaces. The chalcogen passivation of GaAs(100) was achieved using two different procedures. Both procedures result in chalcogen passivated surfaces having almost identical chemical, electronic, and structural properties [19]. In the first procedure As-capped GaAs(100) homoepitaxial layers with a thickness of 2 μm served as substrates. These substrates ($n \approx 10^{18}$ cm^{-3}) were cleaned by annealing at 380 °C for 15 min under UHV conditions resulting in a c(4 × 4) surface reconstruction. Thereafter Se was deposited at 340 °C by thermal decomposition of $SnSe_2$ followed by an annealing process at 400 °C. A (2 × 1) Se-terminated GaAs surface was then detected by means of LEED. In the second procedure the substrates (Freiberger compound GmbH, Te doped, $n = 2 \times 10^{17}$ cm^{-3}) were degreased by ultrasonic baths in acetone, ethanol, and de-ionized water. S passivation was performed by etching in a diluted solution of S_2Cl_2 and CCl_4 (1:3), followed by rinsing in CCl_4, acetone, ethanol, and de-ionized water for 5 s each. Immediately after the chemical treatment the samples were transferred into the UHV chamber and annealed at 430 °C. This results in the formation of Ga_2S_3-like layer terminated by single S atoms [20]. For comparison some PTCDA films are deposited on hydrogen passivated Si(111). The p-type silicon substrates were cleaned and hydrogen passivated by etching for 2 min in HF(40%). After etching the Si substrates were immediately transferred into the UHV chamber. The base pressure of the UHV system was in all cases approximately 2×10^{-8} Pa.

Onto these surfaces PTCDA and DiMePTCDI were deposited at room temperature by thermal evaporation of pre-purified material. The deposition rate was about 0.3 nm min^{-1} for PTCDA and 0.2 nm min^{-1} for DiMePTCDI. The PTCDA and DiMePTCDI source materials were purchased from Lancaster synthesis and Syntec GmbH, respectively. Both were twice purified by sublimation at 595 and 575 K, respectively, under high vacuum ($\sim 10^{-4}$ Pa).

Spectroscopic ellipsometry measurements were performed using a variable angle spectroscopic ellipsometer (VASE from J A Woollam Co., Inc.) equipped with an auto-retarder and a Xe-lamp source. The ellipsometric angles Ψ and Δ were determined in the spectral range from 0.7 to 5 eV at different angles of incidence and by rotating the thin film samples around the substrate normal, the angle of azimuthal rotation being denoted as γ. The diameter of the light spot on the sample was ∼4.5 mm for the incidence angles used. The ellipsometric angles are related to the complex ratio of the reflection coefficients ρ by the formula $\rho = r_p/r_s = \tan(\Psi)e^{i\Delta}$. Here, r_p and r_s are the reflection coefficients of the amplitude of the electric field vector polarized parallel and perpendicular to the plane of incidence, respectively [21].

AFM [22] images were obtained with a commercial microscope (Nanotec Electronica S.L., Spain) equipped with Olympus-type cantilevers having 15 nm nominal radius, a spring constant of 1 N m^{-1}, and a resonance frequency of 78 kHz. AFM images were recorded in non-contact tapping mode using the conditions described in detail elsewhere [23]. Typically, the microscope was operated in ambient conditions at rather low relative humidity of 30%.

NEXAFS spectroscopy was performed at the PM1 and RGBL beamlines of the synchrotron light source BESSYII for the PTCDA and DiMePTCDI samples, respectively. The data were recorded in total yield mode and the light incidence angle α_i was varied between normal and near grazing incidence, i.e. between 0° and 70° (see figure 5). Spectra of a 100 nm thick Ag film were taken for normalization purposes.

The IR spectra were recorded using a Fourier transform infrared (FTIR) spectrometer Bruker IFS 66. Reflectance measurements with p and s polarized light at the extreme angles of incidence α_i (20° and 60°) were performed in the spectral range from 700 to 2000 cm^{-1} and rotating the GaAs(100) substrate stepwise by an angle γ around its normal. The spectral resolution was better than 2 cm^{-1} and the size of the IR beam focused on the sample varied between 2 and 4 mm as a function of the incidence angle.

Raman measurements were performed with a Dilor XY 800 triple monochromator spectrometer equipped with a CCD detector. As the excitation energy the 2.54 eV (488 nm) emission line of an Ar^+ laser was chosen which is resonant with the first main absorption band of both molecules. The films were measured in a backscattering geometry with a spectral resolution of 2.5 cm^{-1}. The incident beam having a power of 30 mW was focused onto a spot of ∼300 μm in diameter.

3. Results and discussion

3.1. Spectroscopic ellipsometry

From ellipsometric measurements the components of the refractive index and extinction coefficient in different directions with respect to the substrate and their dependence on energy, the film thickness and surface roughness are determined. The estimation of the optical constants for PTCDA and DiMePTCDI films is needed for the subsequent evaluation of IR spectra.

In figure 2 the imaginary part $\mathrm{Im}\langle\varepsilon\rangle$ of the effective dielectric function $\langle\varepsilon\rangle = \sin^2\Phi + \sin^2\Phi\tan^2\Phi[(1-\rho)/(1+\rho)]^2$ of a 120 nm thick DiMePTCDI sample is displayed for [011] and [0$\bar{1}$1] azimuthal orientations. The effective dielectric function is influenced by the optical properties of the film, its thickness, the dielectric function of the substrate, and the angle of incidence.

$\mathrm{Im}\langle\varepsilon\rangle$ as presented in figure 2 shows large differences for measurements taken at the same angle of incidence, but with different azimuthal orientations of the sample. Interference induced features below 2 eV can be seen for the [0$\bar{1}$1] direction, but not for the [011] direction.

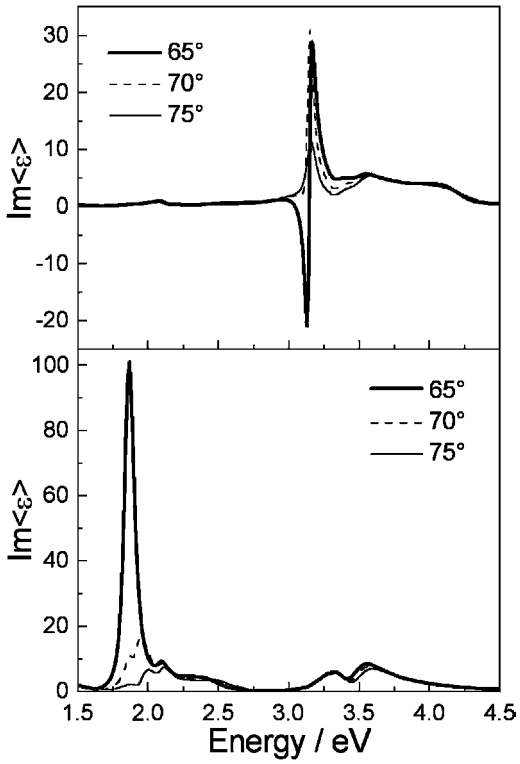

Figure 2. The imaginary part of the effective dielectric function of a 120 nm thick DiMePTCDI film grown on a S passivated GaAs(100) surface. Data are presented for different angles of incidence and different azimuths. The plane of incidence is parallel to the [011] direction (upper figure) and to the $[0\bar{1}1]$ direction (lower figure), respectively.

The strongest feature seen in the case of the $[0\bar{1}1]$ azimuth at 1.8 eV is attributed to interference since the onset of optical absorption is above 2 eV as can be seen in figure 3. DiMePTCDI is strongly absorbing between 2 and 3 eV. In Im$\langle\varepsilon\rangle$ interference induced features are much more pronounced than absorption features. The strong feature at 3.2 eV (the E_1 gap of GaAs) measured for the [011] azimuth showing a derivative-like shape for 65° incidence angle and negative values for the Im$\langle\varepsilon\rangle$ is also induced by interference. These results clearly indicate a very strong in-plane optical anisotropy for DiMePTCDI films.

On the other hand, the anisotropy in the plane parallel to the substrate is very small for PTCDA on GaAs(100) [24]. The imaginary parts of the effective dielectric function for the [011] and $[0\bar{1}1]$ directions differ only slightly. On H passivated Si(111) the absence of an azimuthal dependence indicates in-plane isotropy.

For the extraction of the complex refractive index components the ellipsometry data were evaluated describing each sample by a layer model: substrate/optically anisotropic thin film/surface roughness. For the substrates tabulated database values for the optical constants were used [25]. The low in-plane anisotropy of PTCDA on GaAs was neglected since it lies within the error limit of the following evaluation procedure. Consequently, the thin PTCDA films are modelled as being optically uniaxial and isotropic in the substrate plane.

In addition, film thickness and anisotropic optical constants are determined using a multiple-sample analysis procedure [3]. For this purpose sets of three PTCDA layers with different thicknesses were prepared under the same growth conditions but with different growth

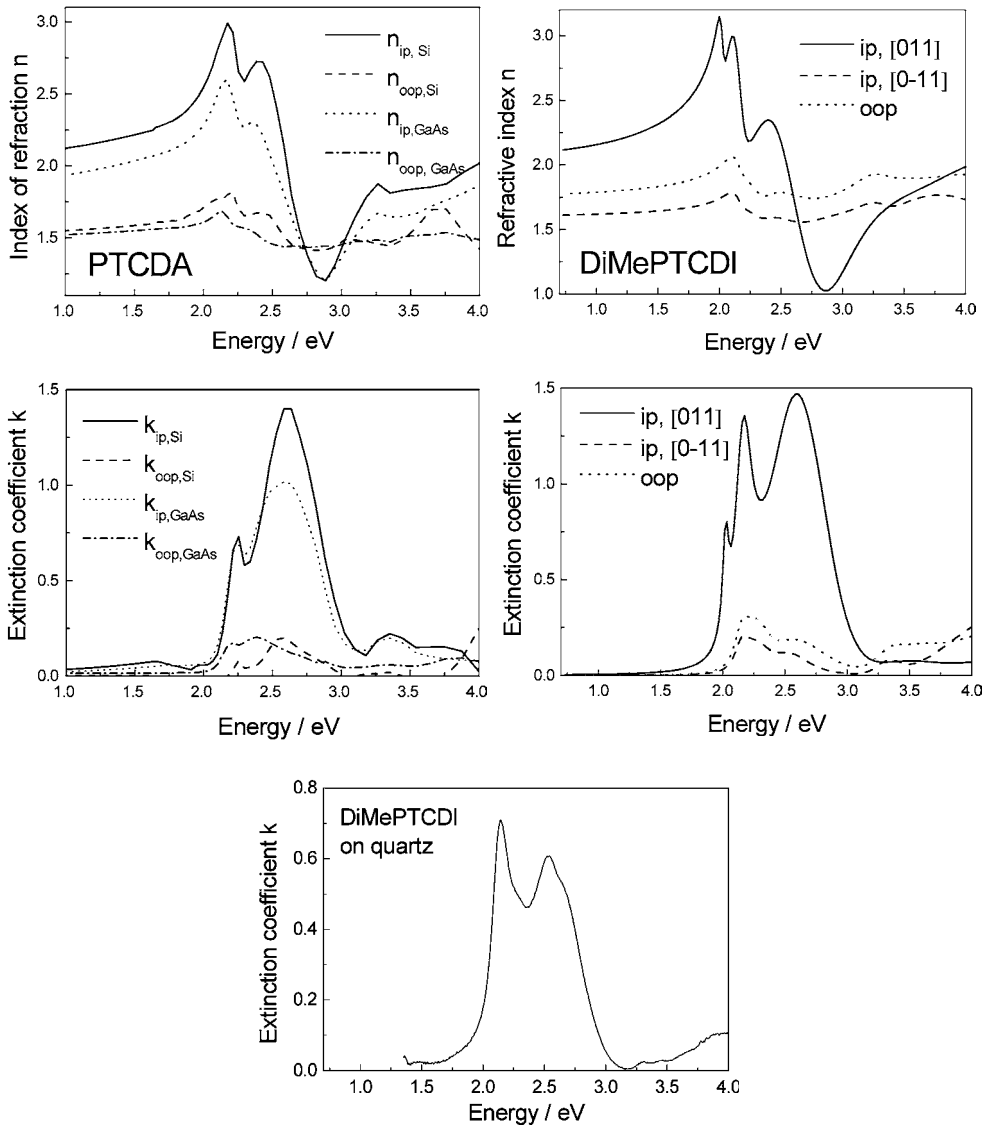

Figure 3. The optical constants of PTCDA films on Se–GaAs(100) and on H–Si(111) (left side) and of DiMePTCDI films on S–GaAs (100) (right side). For comparison the extinction coefficient of an isotropic layer is presented. The notation ip and oop stands for in-plane and out-of-plane, respectively.

times on GaAs and on Si substrates. During the fit procedure the VASE data of all three samples on the same kind of substrate are calculated simultaneously with the optical constants of all the layers being coupled and so varied in the same way.

In contrast to the case for PTCDA, for DiMePTCDI layers on GaAs the observed strong in-plane anisotropy has to be considered additionally. Therefore, a model capable of describing an optically biaxial layer was applied. For the calculations three data sets measured in anisotropic mode at different azimuthal orientation of the same DiMePTCDI sample were coupled and so fitted together [3].

In a first step the transparent spectral range was chosen for the determination of film thickness and surface roughness. Simultaneously, the thicknesses and values for the refractive index components with respect to the Cartesian axes in the substrate plane and normal to it are calculated. In the absorption free low energy range the wavelength dependence of each refractive index was described by a Cauchy dispersion formula: $n = A_n + B_n/\lambda^2 + C_n/\lambda^4$, where A_n, B_n, and C_n are the Cauchy parameters and λ is the wavelength of light.

In addition to film thickness and surface roughness as well as Cauchy parameters for each refractive index, the procedure yields the orientation of optical axes for the biaxial DiMePTCDI film.

The next step of analysis is the determination of complex optical constants in the remaining spectral range. Therefore, the thickness and surface roughness of the films were fixed and starting from the lower energy side a point-to-point fit was carried out resulting in parameter sets of optical constants in each direction.

In a last step a model was built describing the optical constants of the DiMePTCDI film by a set of Gaussian functions, again keeping the thickness and surface roughness constant.

Figure 3 shows the complex refractive indices for PTCDA parallel (ip) and perpendicular (oop) to the substrate plane as a function of energy for the Si and GaAs sample sets.

The thickness and surface roughness for the films on silicon are determined as 212.8 nm/7.9 nm, 80.6 nm/8.0 nm, and 25.5 nm/1.9 nm. The thickness and roughness on GaAs are 77.3 nm/2.2 nm, 28.1 nm/0 nm, and 14.6 nm/ 2.8 nm.

To evaluate the reliability of the results the 90% confidence limits for the optical constants on PTCDA were determined. The 90% confidence limits of the four constants lie between 0.005 and 0.02 in the transparent range and around 0.04 in the spectral range above 1.9 eV.

Comparing the data sets for PTCDA on GaAs and Si, respectively, the line shapes are similar, but lower values for the refractive index for PTCDA on GaAs, especially for the in-plane component, are evident indicating a difference in microstructure and density, with the data for PTCDA on Si being more characteristic for 'bulk' PTCDA. The lower values of the refractive index for PTCDA on GaAs are in agreement with the island-like structure observed for thinner films. As for the refractive index, the extinction coefficient for PTCDA on Si is larger than for PTCDA on GaAs. Furthermore, the in-plane extinction coefficients are much larger than the out-of-plane ones.

The extinction coefficient k in the substrate plane shows a double feature with a smaller sharp peak at 2.25 eV (535 nm), a broader main peak at 2.63 eV (478 nm), and a weaker feature at 3.38 eV (370 nm). These features are assigned to the transitions S0–S1 (HOMO–LUMO), S0–S1 with vibronic progression [26], and S0–S2 (the next highest dipole allowed transition) [27].

The optical constants obtained from a 120 nm thick DiMePTCDI film on S–GaAs(100) are likewise displayed in figure 3. For the refractive index the highest anisotropy is detected for the two distinct directions in the sample plane. The out-of-plane index value in the low energy range lies in between. In the near IR region at 0.7 eV values for the refractive index of 2.11 and 1.62 are determined for in-plane components and 1.78 for the out-of-plane component. These values are relevant for the subsequent analysis of IR spectra.

The larger extinction coefficient k in the substrate plane shows a sharp double feature at 2.19 eV and a broader main peak at 2.6 eV, and weak features above 3 eV. These features are assigned to the transitions S0–S1 (HOMO–LUMO) and S0–S1 with vibronic progression in analogy with the case for PTCDA. The extinction coefficient obtained from a 50 nm thick isotropic film on quartz is likewise displayed in figure 3. This sample which is isotropic due to a random orientation of molecules only exhibits two peaks. This might be a hint that the first peak of the anisotropic sample at 2 eV is an artefact caused by interference. Figure 2 supports

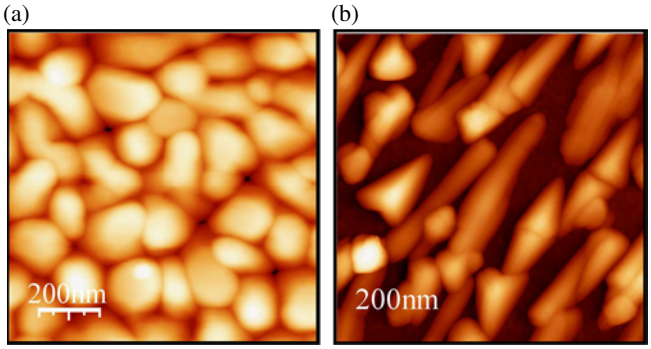

Figure 4. AFM images of PTCDA (a) and DiMePTCDI films (b) grown on S–GaAs(100). (This figure is in colour only in the electronic version)

this interpretation. However, further measurements using samples with different thicknesses are required to clarify the origin of this feature.

3.2. AFM investigations

Deposition of PTCDA on S passivated GaAs(100) at room temperature leads to PTCDA aggregates with an average diameter of 100 nm. Figure 4(a) shows a topographic AFM picture (1 μm $\times$ 1 μm) taken from a 30 nm thick PTCDA film. X-ray diffraction investigations performed on these samples revealed only one diffraction peak corresponding to the (102) plane of the PTCDA crystal indicating a predominant orientation of these plane parallel to the substrate surface. In the case of DiMePTCDI on S passivated GaAs(100), deposition at room temperature leads to the formation of ribbon-like crystals. In figure 4(b) a topographic AFM picture (1 μm $\times$ 1 μm) corresponding to a nominal coverage of 20 nm is shown. The crystals in the image are aligned with the edges of the cleaved substrate. Their morphology supports the strong optical in-plane anisotropy of DiMePTCDI films derived from VASE.

3.3. NEXAFS

In NEXAFS spectroscopy, absorption of the tunable synchrotron radiation takes place by exciting electrons from core shells into unoccupied states. Considering π^* unoccupied states in perylene derivatives, maximum intensity is expected when the electric field vector of the synchrotron light is polarized perpendicular to the molecular plane [28].

In figure 5 the dashed arrow indicates the direction of transition dipoles involved in an excitation from the 1s core level to the π^* states. The absorption intensity can be expressed as a function of the angle between the electric field vector and the direction of the dipole transition. More accurately, the intensity is proportional to $\cos^2(\theta + \alpha_i - 90°)$ where θ is the tilt angle of the molecular plane and α_i is the angle of incidence.

Figure 6(a) presents selected C 1s NEXAFS spectra of a 20 nm thick PTCDA film grown on S–GaAs(100) for three different angles of incidence. The lower photon energy features near 280 eV correspond to π^* states. Here, π^* resonances are negligible for an incidence angle of 0° (perpendicular to the sample surface) and increase showing maximum intensity for large angles of incidence (70°). The increase in intensity of the π^* resonances with increasing angle of incidence together with additional data for the oxygen edge provide clear evidence for the parallel orientation of the molecular plane with respect to the substrate surface [29].

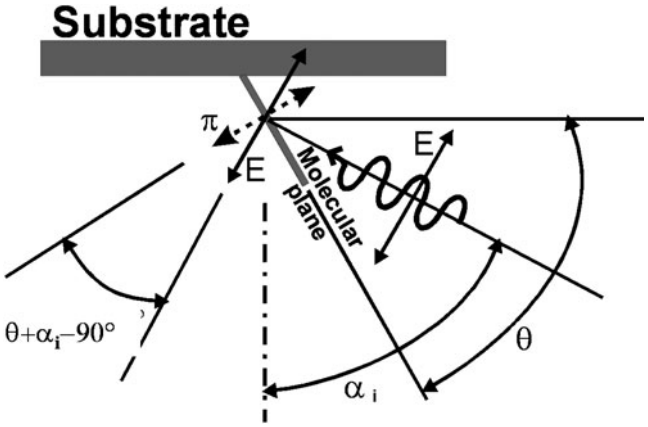

Figure 5. The geometry of the NEXAFS measurement.

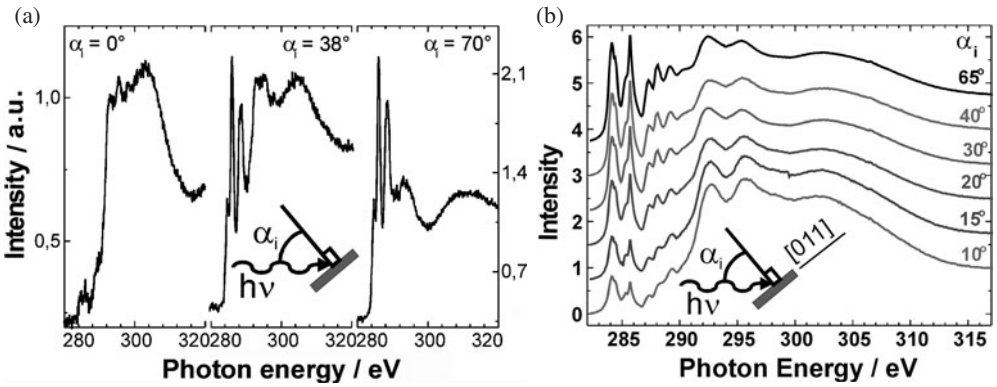

Figure 6. Evolution of the π^* resonances with the incidence angle I for (a) PTCDA and (b) DiMePTCDI grown on S–GaAs substrate.

The evolution of DiMePTCDI NEXAFS spectra as a function of the angle of incidence is shown in figure 6(b) for a 10 nm thick film on S–GaAs(100). All the spectra were normalized with respect to the intensity at 315 eV photon energy. For background subtraction, the NEXAFS spectrum of a bare S–GaAs(100) sample was employed. The σ^* resonances (near 300 eV photon energy) are clearly distinguished form the π^* ones (below 287 eV) due to their asymmetric line shape [28]. An increase in the intensity of the π^* resonances is observed with increasing incidence angle; σ^* resonances, however, show an opposite trend.

The tilt angle of the molecular plane θ, and the projection χ of the long axis of the molecular plane onto the substrate can be obtained from a simulation of the experimental intensities. The intensity ratio for the bands related to π^* resonances is presented in figure 7 (symbols) as a function of the incidence angle for two azimuthal directions of the sample: when the plane of incidence contains the [011] (figure 7(a)) and [0$\bar{1}$1] (figure 7(b)) directions of the S–GaAs(100) substrate. The simulation is performed using a model that assumes the same orientation for all molecules, and the relationship between the NEXAFS intensity and the angles describing the molecular orientation is obtained following the algorithm proposed in [28]. The best fits to the experimental data are also presented in figure 7. An average tilt angle of $\theta = 56^\circ \pm 5^\circ$ of the molecular plane is obtained while for the in-plane projection

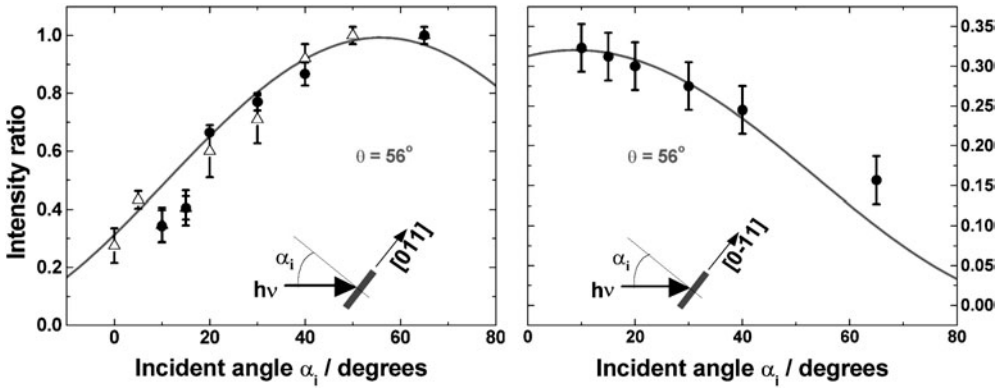

Figure 7. Experimental (symbols) and calculated (curves) intensity ratios for π^* resonances as a function of the incidence angle. Different symbols indicate data from different samples.

an angle of $\chi = -7^\circ \pm 3^\circ$ with respect to the [011] axis of the GaAs substrate is evaluated. The orientation of DiMePTCDI molecules on S–GaAs(100) will now be further evaluated by considering IR and Raman spectroscopy results.

3.4. Assignment of vibrational properties

For quantitative analysis of the polarized response recorded in IR and Raman spectroscopies the knowledge of the vibrational mode character and their symmetry is essential.

In order to make an assignment of Raman and IR features to vibrational modes we have carried out density functional calculations in the Gaussian'98 package [30] at the B3LYP level of theory using the standard 3-21G basis set.

The point symmetry group of the PTCDA molecule is D_{2h}. PTCDA has 38 atoms and hence exhibits 108 internal modes. Those that are symmetric with respect to the centre of inversion (labelled with g) are usually Raman active and those that are anti-symmetric (labelled with u) show IR activity. The representation of the internal modes is

$$\Gamma_{\mathrm{PTCDA}} = 19A_g + 18B_{1g} + 10B_{2g} + 7B_{3g} + 10B_{1u} + 18B_{2u} + 18B_{3u} + 8A_u.$$

DiMePTCDI consists of 46 atoms, the point symmetry group of the molecule being C_{2h} or C_{2v}, for the geometry with an inversion centre and that without, respectively.

There are 132 internal molecular vibrational modes. In the case of C_{2h} symmetry, 66 of them are Raman active ($44A_g + 22B_g$) and 66 are IR active ($23A_u + 43B_u$). For the C_{2h} symmetry, there are $44A_g + 22B_g + 23A_u + 43B_u$ irreducible representations, with the corresponding vibrational modes being either Raman or IR active. Due to the similarity in the calculated frequencies of modes for the two point groups the geometry with C_{2h} symmetry will be considered for ease of comparison with PTCDA.

3.5. Infrared spectroscopy

A comparison between calculated IR modes of PTCDA and DiMePTCDI for a single molecule and measured ones and their assignments are given in table 2. In this IR section the molecular coordinates displayed in figure 1 are presented for simplification without indices: $x_m = x$, $y_m = y$, and $z_m = z$.

IR measurements on PTCDA/S–GaAs(100) samples reveal isotropy in the substrate plane. The ratio of the in-plane molecular modes with respect to the out-of-plane ones is similar to

Table 2. Comparison between the experimental frequencies of the IR modes for PTCDA and DiMePTCDI films on S–GaAs(100) and calculated properties for the corresponding isolated molecules.

Experiment (cm^{-1})		B3LYP: 3-21G (cm^{-1})		Symmetry		Dominant character	
PTCD A	DiMePTCDI	PTCDA	DiMePTCDI	PTCDA	DiMePTCDI	PTCDA	DiMePTCDI
733	743	764	786	$B_{3u}(z)$	$A_u(z)$	$\delta_{O=C-C} + \delta_{C-O-C} + \delta_{C-C-C}$, oop	$\delta_{C-H} + \delta_{C-C-C}$, oop
809	809	853	859	$B_{3u}(z)$	$A_u(z)$	$\delta_{C-H} + \delta_{C-C-C}$, oop	$\delta_{CH_3} + \delta_{C-C-C}$, oop
939		947		$B_{1u}(y)$		$\nu_{C-C} + \nu_{C-O}$	
1017, 1024	1022, 1053	1040	1032	$B_{1u}(y)$	$B_u(x)$	$\nu_{C-O} + \nu_{CC}$	$\delta_{C-H} + \nu_{ring} + \delta_{CH_3}$
1236	1237	1256	1260, 1265	$B_{1u}(y)$	$B_u(y)$; $B_u(x)$	$\delta_{C-H} + \nu_{C-C}$	$\delta_{C-H} + \delta_{ring} + \delta_{CH_3}$; $\delta_{C-H} + \delta_{C-N-C}$
1300	1285	1309	1317	$B_{2u}(x)$	$B_u(y)$	$\delta_{C-H} + \nu_{C-C}$	$\delta_{C-H} + \delta_{C-N-C} + \delta_{CH_3}$
	1350, 1358		1346		$B_u(x)$		$\nu_{C-C} + \delta_{C-N-C} + \delta_{C-H} + \delta_{CH_3}$
1407	1400	1439	1372	$B_{2u}(x)$	$B_u(x)$	$\delta_{C-C} + \nu_{C-C}$	$\delta_{C-H} + \delta_{CH_3} + \nu_{C-N}$
					$B_u(x)$;		$\delta_{C-H} + \nu_{C-C}$;
	1436, 1449		1438, 1456;		$B_u(x)$,		$\delta_{C-H} + \delta_{ring} + \delta_{CH_3}$
			1483		$B_u(x)$		CH_3 umbrella def.
1594	1577, 1593	1618	1617	$B_{2u}(x)$	$B_u(x)$	$\nu_{C-C} + \delta_{C-H}$	$\nu_{C-C} + \delta_{C-H}$
1731, 1743	1658, 1665	1756	1678	$B_{1u}(y)$	$B_u(y)$	$\nu_{C=O}$	$\nu_{C=O}$
1771, 1778	1692, 1696	1796	1715	$B_{2u}(x)$	$B_u(x)$	$\nu_{C=O}$	$\nu_{C=O} + \delta_{CH_3}$

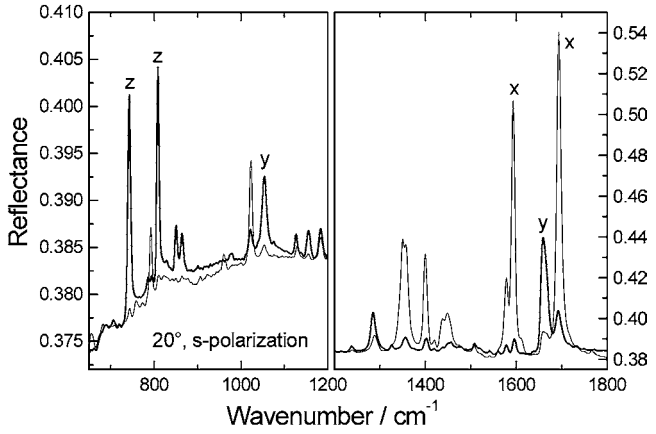

Figure 8. Infrared reflection spectra of DiMePTCDI with the [011] direction (thick curve) and [0$\bar{1}$1] direction (thin curve) parallel to the plane of incidence.

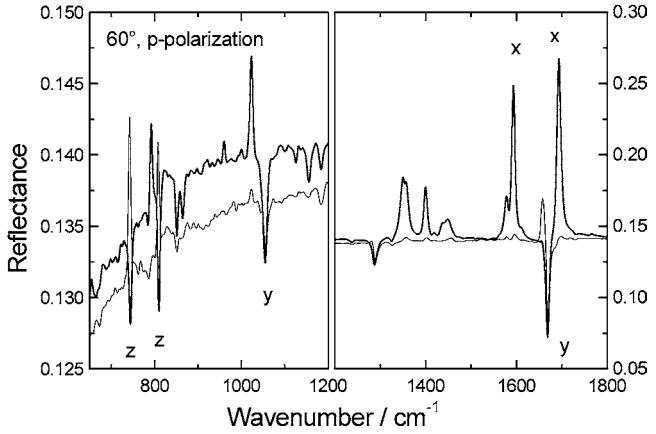

Figure 9. Infrared reflection spectra of DiMePTCDI measured at 60° angle of incidence with p polarized light.

that observed for PTCDA/Si(111). Quantitative analysis of this ratio reveals that the molecular planes of the PTCDA molecules form an average angle of ∼9° with respect to the Si(111) substrate plane [31].

The results of IR measurements for 120 nm DiMePTCDI on S–GaAs(100) are given in figures 8 and 9. Figure 8 shows the IR reflectance spectra measured in s polarization at 20° angle of incidence with the [011] (thick curves) and [0$\bar{1}$1] (thin curves) directions of the substrate parallel to the plane of light incidence; i.e. the electric field is parallel to the [0$\bar{1}$1] and [011] directions. For this near normal incidence it is obvious that the s polarized spectra in [011] and [0$\bar{1}$1] directions show totally different absorption features. From these spectra we can again derive without any calculation that the film has a strong in-plane anisotropy. By comparing the experimental frequency and intensity with calculated ones (see table 2) the strongest features measured in the [0$\bar{1}$1] direction can be assigned to vibrations along the *x* direction of the molecule. The contribution of features related to other molecular directions is small. Dominance of features related to vibrations in *y* and *z* directions of the molecule,

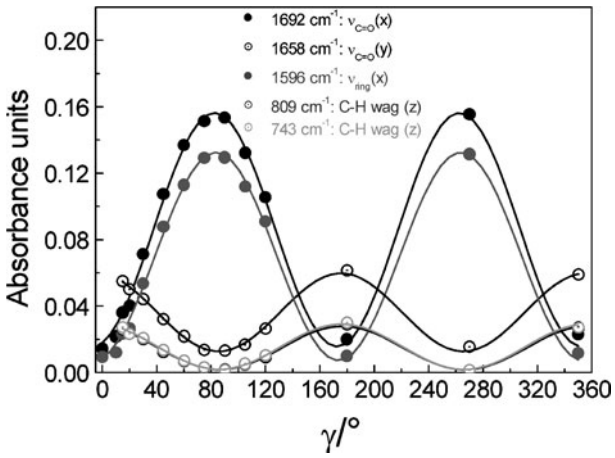

Figure 10. Intensities of x, y and z features of DiMePTCDI as a function of azimuth angle for near normal incidence. Measurements are done with s polarized light.

on the other hand, is observed in the [011] direction spectra. The characteristic features used for further evaluation are marked with x, y, or z.

From the spectra in figure 8 we can derive that the DiMePTCDI molecules are preferentially arranged with their x axis in the [011] direction, the direction of the electric field vector, while measuring in s polarization when the $[0\bar{1}1]$ direction lies in the plane of incidence. The measurements at 60° angle of incidence for s polarized light (not shown) are similar to those in figure 8 and confirm the in-plane anisotropy.

Additional information about the vibrational modes in the [100] direction can be extracted from the 60° measurements using p polarized light. The spectra are presented in figure 9. The electric field vector lies in the incidence plane. For the measurement in the [011] direction (thick curve) we see as expected the x features pointing up and additional y and z features pointing down, including information about the [100] direction with respect to the substrate. In the $[0\bar{1}1]$ direction (thin curve) the contribution of x features is negligibly small. Only z features pointing up and y features pointing down are perceptible. The p polarized spectra in figure 9 clearly indicate that the molecular planes are tilted with respect to the substrate surface.

Figure 10 shows the results of measurements performed at near normal incidence turning the sample around its surface normal by an angle γ starting with the plane of incidence containing the [011] direction of the substrate. The behaviour of the DiMePTCDI bands can be well described by a $\cos^2$ function as shown in figure 10. The intensity maxima of y and z features are shifted by an angle of about 90° with respect to those of the x features. Maxima are observed at angles $\gamma_x = 7°$ and $\gamma_y = \gamma_z = 94°$. The ratios of the maximum and minimum in-plane intensity values are presented in table 3.

With the minimum I_{ax} and maximum values I_{bx} of x features, a coarse evaluation can be performed using the formula given in [32] for the determination of the dichroic ratio D_x. The formula derived for transmission spectra is applied here to reflection spectra of a 120 nm thick film showing absorption features similar to those which are characteristic for transmission spectra. We obtain

$$D_x = \frac{I_{bx}}{I_{ax}} = \frac{n_a}{n_b} \cot^2 \chi. \tag{1}$$

Table 3. Dichroic ratios observed for selected IR modes of DiMePTCDI.

		Dichroic ratio	
Wavenumber (cm^{-1})	Character	I_a/I_b	I_b/I_a
743	z	15.8	
809	z	16.5	
1054	y	4.5	
1596	x		18.1
1658	y	4.7	
1692	x		10

Here the refractive indices $n_b = 2.11$ and $n_a = 1.62$ determined previously by spectroscopic ellipsometry in the near IR range are employed. The a and b directions defined via the minimum and maximum intensity values in figure 10 almost coincide with the directions of the electric field vector during measurement. They correspond to the [011] and [0$\bar{1}$1] directions of the substrate, respectively.

Furthermore we can estimate the ratios

$$D_y = \frac{I_{ay}}{I_{by}} \qquad \text{and} \qquad D_z = \frac{I_{az}}{I_{bz}}. \tag{2}$$

Under the assumptions that the long axes of the molecules are parallel to the sample surface and that the molecules have a good preferential orientation with their long axis parallel to the [011] direction of the sample we can determine in a further approach an average tilt angle θ of the molecular plane with respect to the sample surface from the quotient of D_y and D_z:

$$\tan^2(1-\theta) = \frac{D_y}{D_z}. \tag{3}$$

With the quantities from table 3 a tilt angle of $\theta = 62^\circ \pm 6^\circ$ is calculated. The angle is larger compared to that from NEXAFS spectroscopy. Sources of error are the low intensity of IR features, the angular spread of IR light, and the assumption that the x axis of molecules lies parallel to the sample surface.

The angle χ determined from equation (1) should be the same for all x modes. However, with equation (1) different angles χ are calculated from the different dichroic ratios D_x of the ring band at 1596 cm^{-1} and the side-group band at 1692 cm^{-1}. The deviation is too high to be explainable by the experimental error alone. Further investigations are required for a better understanding.

3.6. Raman spectroscopy

PTCDA films exhibit a very weak dependence of the Raman scattered intensity upon the azimuthal rotation of the sample around the substrate normal supporting the in-plane isotropy described in the previous ellipsometry, NEXAFS, and IR spectroscopy sections. For DiMePTCDI the situation is entirely different. First of all the Raman spectra provide evidence for the crystalline nature of films through the presence of external molecular modes (phonons) [33]. The number and frequency positions of these phonons correspond to those detected in a single crystal for which XRD measurements proved a crystalline composition with monoclinic symmetry. Recalling the ribbon-like structure evidenced by AFM it can be concluded that the films are polycrystalline.

Considering the long-range ordering of DiMePTCDI films a quantitative analysis of the polarization dependent Raman spectra will be attempted in the following in order to assess the molecular orientation.

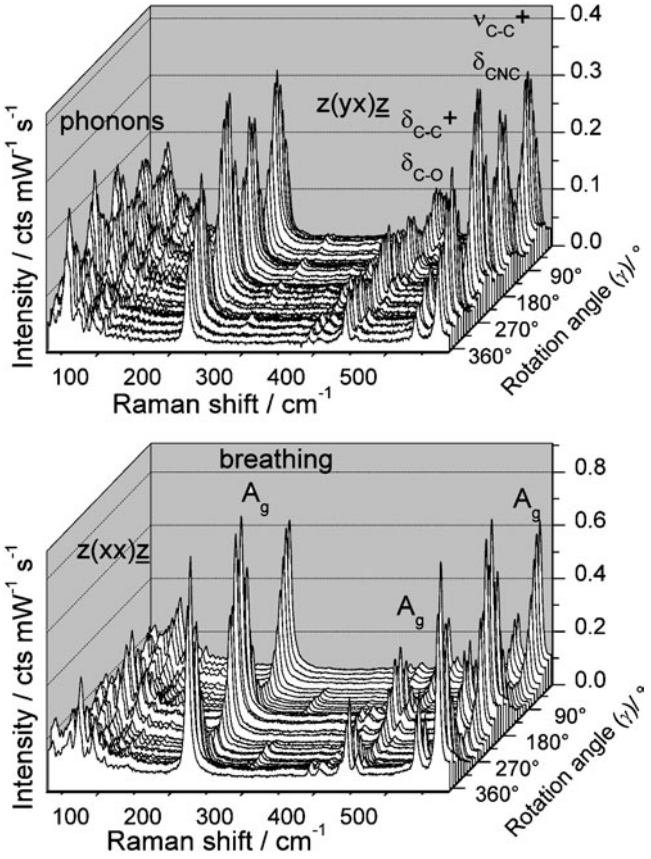

Figure 11. Low frequency Raman spectra of DiMePTCDI upon rotation of the sample around its normal (with angle γ). Upper and lower spectra are recorded in crossed and parallel polarization, respectively.

For this purpose the 120 nm DiMePTCDI film was rotated clockwise in angular steps of 10°. A fixed laboratory coordinate system (x, y, z) was defined such that the z axis is parallel with the direction of the incident beam and perpendicular to the sample surface. The x axis was defined to be parallel to the direction of the polarization analyser. The electric field vector of the incident radiation was either parallel to x or perpendicular to it (parallel to the y axis). The laboratory axes coincide with the substrate axes ($x = x_s = [011]$, $y = y_s = [0\bar{1}1]$, $z = z_s = [100]$) when $\gamma = 0°$. Two polarization configurations were used for each sample position. In the Porto notation $z(xx)\underline{z}$ and $z(yx)\underline{z}$ denote the cases when the incident electric field vector of scattered light is parallel/perpendicular to that of the analysed light (parallel/crossed polarization configuration).

The spectra obtained upon sample rotation are shown in figure 11. The Raman intensities of A_g modes vary with a period of 180° and 90° in parallel and in crossed polarization, respectively. The maximum response in parallel polarization for the A_g modes takes place when the electric field vectors are parallel to the [011] direction of the substrate ($\gamma = 0°$, 180°). This indicates a good ordering of the molecules with a preferred orientation of their x_m axis close to the [011] substrate axis, in agreement with the NEXAFS and IR results.

The density functional methods employed for the assignments of vibrational modes served also for determination of the Raman tensor specific for the A_g modes:

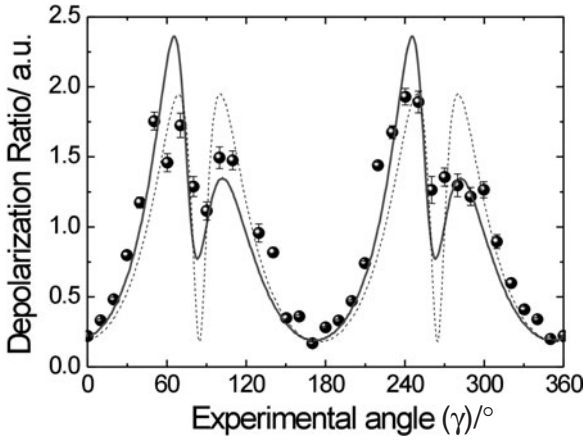

Figure 12. Experimental (symbols) and simulated (curves) depolarization ratios of the breathing mode at ∼221 cm^{-1} obtained upon rotation around sample normal with the angle γ for a DiMePTCDI film.

$$A_g^m = \begin{pmatrix} a & d & 0 \\ d & b & 0 \\ 0 & 0 & c \end{pmatrix}. \tag{4}$$

As an example, the tensor components obtained for the lowest frequency internal mode (∼221 cm^{-1}) have the following values: $a = 1$, $b = 0.04$, $c = 0$, and $d = -60$, with the tensor elements being normalized with respect to the a component. The mode considered has a breathing character, mainly along the long molecular axis (x_m). One has to keep in mind that this was calculated for an isolated molecule under non-resonant conditions.

The symmetry of the highest occupied molecular orbital (HOMO) of DiMePTCDI is A_u, and that of the lowest unoccupied molecular orbital (LUMO) is B_g. Therefore a resonant Raman effect involves a HOMO–LUMO transition with an electronic transition dipole oriented along the x_m axis. The effect of resonant excitation is taken into consideration by neglecting the off-diagonal components ($a = 1$; $b = 0.04$; $c = d = 0$).

The twofold Davydov frequency splitting expected due to the coupling of the two molecules in the unit cell is so small for the internal modes of DiMePTCDI that it lies at the experimental detection limit both for Raman and IR active modes. Therefore, any perturbation of the molecular Raman tensor elements induced by intermolecular interactions can be neglected.

A concept widely used in the literature dedicated to quantitative analysis of sample polarization response is the depolarization ratio [34]. This is defined as the ratio between the Raman signals obtained in the crossed polarization configuration to that obtained in the parallel configuration:

$$\mathrm{Dep} = \frac{I_{yx}}{I_{xx}}. \tag{5}$$

The experimental depolarization ratio of the 221 cm^{-1} mode is shown as a function of rotation angle γ by symbols in figure 12.

In order to extract the geometrical arrangement of the molecules from the depolarization ratios there are three coordinate systems to be taken into account: molecular (x_m, y_m, z_m), substrate (x_s, y_s, z_s), and laboratory (x, y, z). Two consecutive transformations are required to transform the molecular Raman tensor to the laboratory reference. The first orthogonal

transformation can be applied using the Euler angles (φ, θ, ψ). This method was previously employed by Aroca *et al* [35] for the Raman study of a highly symmetric molecular system (InPcCl, point group D_{4h}). The transformation from the molecular to the substrate coordinate system is described by

$$R = R(\varphi)R(\theta)R(\psi) \tag{6}$$

where

$$R(\varphi) = \begin{pmatrix} \cos\varphi & \sin\varphi & 0 \\ -\sin\varphi & \cos\varphi & 0 \\ 0 & 0 & 1 \end{pmatrix}, \qquad R(\psi) = \begin{pmatrix} \cos\psi & \sin\psi & 0 \\ -\sin\psi & \cos\psi & 0 \\ 0 & 0 & 1 \end{pmatrix},$$

and

$$R(\theta) = \begin{pmatrix} 1 & 0 & 0 \\ 0 & \cos\theta & \sin\theta \\ 0 & -\sin\theta & \cos\theta \end{pmatrix}. \tag{7}$$

The molecular Raman tensor will be transformed according to

$$\mathrm{A}_\mathrm{g}^\mathrm{s} = R\mathrm{A}_\mathrm{g}^\mathrm{m}R^{-1} \tag{8}$$

where R^{-1} is the transpose of matrix R.

The second transformation is from the substrate to the laboratory coordinate system and implies a clockwise rotation around the substrate normal (z_s) with the angle γ.

The corresponding rotation matrix is

$$R(\gamma) = \begin{pmatrix} \cos\gamma & \sin\gamma & 0 \\ -\sin\gamma & \cos\gamma & 0 \\ 0 & 0 & 1 \end{pmatrix} \tag{9}$$

and the transformation is described as

$$\mathrm{A}_\mathrm{g} = R(\gamma)^{-1}\mathrm{A}_\mathrm{g}^\mathrm{s}R(\gamma). \tag{10}$$

The Raman intensity is then calculated as

$$I = (\mathbf{e}_\mathrm{s} \cdot \mathrm{A}_\mathrm{g}\mathbf{e}_\mathrm{i})^2 \tag{11}$$

where $\mathbf{e}_\mathrm{i}$ and $\mathbf{e}_\mathrm{s}$ describe the direction of the electric field vectors for the incident and the scattered light, respectively.

A least squares fit of the experimental depolarization ratio was performed using a Levenberg–Marquardt algorithm. The closest match between the calculated depolarization ratios obtained using the one-molecule approximation is represented in figure 12 by the dashed curve. The corresponding set of Euler angles is $(\varphi = -70°, \theta = 53°, \psi = 51°)$, which means that the molecular plane is tilted with respect to that of the substrate by $53° \pm 5°$, and the angle between the projection of x_m onto the substrate plane and the [011] substrate axis is $-7° \pm 5°$. This set of angles is very close to those determined from the NEXAFS and IR measurements (see previous sections). However, even though the main maxima of the experimental data are reproduced well, the steep minima and the equality of height of all maxima indicate that a more complex model is required.

Considering the crystalline nature of the film reflected by the presence of phonons, a natural approach would be to consider two non-interacting molecules whose Raman signals add up. The model was constructed such that the angles between the two molecules in the unit cell are maintained close to the angles reported for the single crystal and only the unit cell is rotated with respect to the substrate by changing the Euler angles. The coordinate system of the unit cell (x_u, y_u, z_u) was chosen such that the x_u and y_u axes are contained in the (102) crystallographic plane. The molecular planes of the two molecules are tilted with +8° and −8°

with respect to the $(x_u y_u)$ plane, and the long axes of the two molecules are rotated by +18° and −18° with respect to the x_u axis.

The lowest deviation between the calculated and the experimental data is provided by the following set of Euler angles: $\varphi = 114° \pm 5°$; $\theta = 56° \pm 4°$, $\psi = 28° \pm 5°$. This means that the crystal (102) plane forms an angle of 56° with the substrate plane, and the projections of the long molecular axis deviate from the [011] direction of the substrate by $\chi_1 = -7° \pm 5°$ and $\chi_2 = -48° \pm 11°$, respectively.

It must be noted that in each of the two models the minima of the depolarization ratio should be very close to zero assuming that the scattered light is totally polarized. In order to reproduce the experimental values in the minima the scattered intensities in parallel and perpendicular configurations had to be mixed by a constant factor D:

$$\mathrm{Dep} = \frac{(1-D)I_{yx} + DI_{xx}}{DI_{yx} + (1-D)I_{xx}}. \tag{12}$$

The parameter D was also optimized during the fitting procedure and for both models the resulting value was $D \sim 0.15$. This parameter describes a depolarization in the light scattered by the sample due to the surface roughness [36, 37], thickness non-uniformity [36], angular spread of the collected beam [36, 37], and eventually due to a spread in the orientation of some molecules from the preferential arrangement.

4. Summary

NEXAFS, IR, and Raman spectroscopies were applied for the determination of the molecular orientation in PTCDA and DiMePTCDI films grown on chalcogen passivated GaAs(100) substrates, and VASE for the determination of macroscopic optical properties displaying the anisotropy due to molecular arrangement on a macroscopic level.

The optical constants of PTCDA determined by VASE in the plane parallel to the substrate plane are rather similar, while much lower values have been determined along the direction perpendicular to it. For DiMePTCDI very large differences were measured along two orthogonal directions in the GaAs substrate plane.

While the PTCDA molecules were found to lie flat on the substrate by means of NEXAFS and previously XRD and IR spectroscopy, a large tilt angle of the DiMePTCDI molecular plane with respect to the GaAs substrate plane and a preferential azimuthal orientation were determined in this work. The tilt and azimuthal angles from NEXAFS, IR, and Raman spectroscopy are summarized in table 4. Figure 13 shows a sketch of the unit cell in the (102) DiMePTCDI crystal plane and the relative orientation with respect to the GaAs substrate. The good agreement between the tilt angles derived from different techniques indicates that each of them is a reliable method. However, the deviation in the azimuthal angle supports the thesis that a one-molecule model is too simple.

The AFM image displaying long-range ordering and the observation of molecular external modes in Raman spectroscopy provide evidence for the crystalline character of the films. Therefore a model taking into account two molecules with relative angular orientation as in a monoclinic crystal is expected to produce more accurate results. Up to now only the Raman data were evaluated with both models. Further analysis of NEXAFS and IR data considering crystallinity will be performed for completing the understanding of molecular orientation in DiMePTCDI/S–GaAs(100) heterostructures.

From the techniques applied, resonant Raman spectroscopy and NEXAFS spectroscopy are best suited to characterizing the molecular orientation in very thin samples (∼1 nm). Thicker samples (∼100 nm) are required for the determination of optical constants by means of

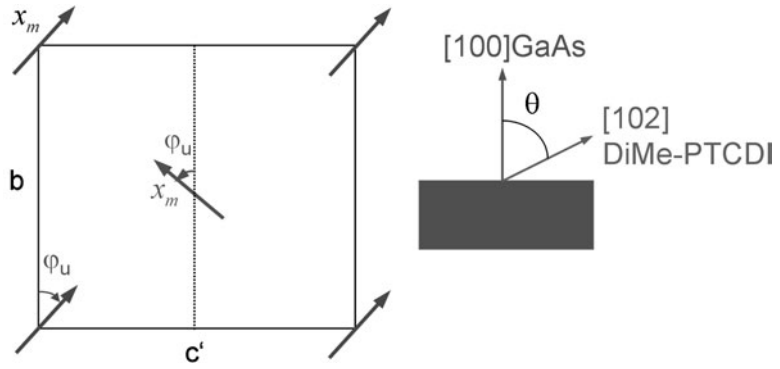

Figure 13. A schematic diagram of the DiMePTCDI unit cell in the (102) crystalline plane (left) and of the relative orientation of the (102) planes with respect to the S–GaAs(100) substrate (right, both defined by the normal direction).

Table 4. Angles defining the orientation of the DiMePTCDI molecules with respect to the S–GaAs(100) substrate as determined by the techniques discussed in this work. The angles θ and χ denote the tilt of the molecular plane with respect to the substrate plane and the angle made by the projection of the long molecular axis on the substrate plane with respect to the [011] direction of the substrate.

	Technique			
			Raman	
Angle (deg)	NEXAFS	IR	One molecule	Two molecules
θ	56 ± 5	62 ± 6	53 ± 5	56 ± 4
χ	-7 ± 3	11.7 ± 3	-7 ± 5	$\chi_1 = -7 \pm 5$ $\chi_2 = -48 \pm 11$

VASE and also for the quantitative analysis of molecular orientation by IR spectroscopy. From the point of view of data evaluation the mathematical formalism for NEXAFS spectroscopy is the simplest. The strength of the Raman model lies in the use of the depolarization ratio which reduces the experimental errors affecting the absolute intensities. However, the weakness of the model is related to the complex formalism employing knowledge of the Raman tensor. The strength of IR spectroscopy lies in the simple detection of anisotropy. With knowledge of the optical constants, the azimuthal angle can be directly derived from the dichroic ratio. Due to the poor access to the direction perpendicular to the substrate surface the accuracy for the IR determination of the tilt angle is relatively low. VASE delivers after a complex evaluation procedure macroscopic optical constants for all directions. From these constants in principle an average molecular orientation can also be calculated using the features assigned to S0–S1 transitions for thicker films with a homogeneous structure.

Acknowledgments

A Paraian and S Park are gratefully acknowledged for performing parts of the ellipsometry and NEXAFS measurements.

The authors involved in the NEXAFS investigations thank the BESSY staff, in particular W Braun, P Bressler, D Vyalikh, for technical assistance and fruitful discussions.

The financial support for this work was provided by the EU funded Human Potential Research Training Network DIODE (Contract No HPRN-CT-1999-00164), by the

Bundesministerium für Bildung und Forschung (BMBF, Grant No 05KS1OCA/1) and by the Graduiertenkolleg, 'Dünne Schichten und nichtkristalline Materialien' at the University of Technology Chemnitz.

References

[1] Forrest S R, Kaplan M L and Schmidt H P 1984 *J. Appl. Phys.* **55** 1492
[2] Zang D Y, So F F and Forrest S R 1991 *Appl. Phys. Lett.* **59** 823
[3] Friedrich M, Wagner Th, Salvan G, Park S, Kampen T U and Zahn D R T 2002 *Appl. Phys.* A **75** 501
[4] Hädicke E and Graser F 1986 *Acta Crystallogr.* C **42** 189
[5] Hädicke E and Graser F 1986 *Acta Crystallogr.* C **42** 195
[6] Klebe G, Graser F, Hädicke E and Berndt G 1989 *Acta Crystallogr.* C **45** 69
[7] Möbus M, Karl N and Kobayashi T 1992 *J. Cryst. Growth* **116** 495
[8] Lovinger A J, Forrest S R, Kaplan M L, Schmidt P H and Venkatesan T 1984 *J. Appl. Phys.* **55** 476
[9] Kendrick C and Kahn A 1997 *J. Cryst. Growth* **181** 181
[10] Hirose Y, Forrest S R and Kahn A 1995 *Phys. Rev.* B **52** 14040
[11] Kampen T U, Salvan G, Tenne D and Zahn D R T 2001 *Appl. Surf. Sci.* **175/176** 326
[12] Nicoara N, Cerrilló I, Xueming D, García J M, García B, Gómez-Navarro C, Méndez J and Baró A M 2002 *Nanotechnology* **13** 352
[13] Das A, Salvan G, Kampen T U, Hoyer W and Zahn D R T 2003 *Appl. Surf. Sci.* **212/213** 413
[14] Lifshitz E, Kaplan A, Ehrenfreund E and Meissner D 1999 *Chem. Phys. Lett.* **300** 626
[15] Yanagi H, Toda Y and Noguchi T 1995 *Japan. J. Appl. Phys.* **34** 3803
[16] Nowakowski R, Seidel C and Fuchs H 2001 *Phys. Rev.* B **63** 195418
[17] Schäfer A H, Seidel C and Fuchs H 1998 *Thin Solid Films* **379** 176
[18] Seidel C, Schäfer A H and Fuchs H 2000 *Surf. Sci.* **459** 310
[19] Zahn D R T, Kampen T U, Hohenecker S and Braun W 2000 *Vacuum* **57** 139
[20] Kampen T U, Zahn D R T, Braun W, Gonzáles C, Benito I, Ortega J, Jurczyszyn L, Blanco J M, Pérez R and Flores F 2003 *Appl. Surf. Sci.* **212/213** 850
[21] Azzam R M A and Bashara N M 1997 *Ellipsometry and Polarized Light* (Amsterdam: North-Holland)
[22] Binnig G, Quate C F and Gerber C 1986 *Phys. Rev. Lett.* **56** 930
[23] Moreno-Herrero F, de Pablo P J, Colchero J, Gómez-Herrero J and Baró A M 2000 *Surf. Sci.* **453** 152
[24] Kampen T U, Paraian A M, Rossow U, Park S, Salvan G, Friedrich M and Zahn D R T 2001 *Phys. Status Solidi* **181** 1307
[25] Adachi S 1999 *Optical Constants of Crystalline and Amorphous Semiconductors* (Dordrecht: Kluwer–Academic)
[26] Scholz R, Vragovic I, Kobitski A Yu, Salvan G, Kampen T U, Schreiber M and Zahn D R T Organic nanostructures: science and applications *Proc. Scuola Int. Fizika ('Enrico Fermi', Course CXLIX)* (Amsterdam: IOS Press) pp 379–403
[27] Hoffmann M 2000 *PhD Thesis* Dresden University
[28] Stöhr J 1996 *NEXAFS Spectroscopy* (Berlin: Springer)
[29] Park S 2002 *PhD Thesis* Chemnitz University
[30] Frisch M J *et al* 1998 *Gaussian 98 (Revision A.1)* (Pittsburgh, PA: Gaussian)
[31] Scholz R, Friedrich M, Salvan G, Kampen T U and Zahn D R T 2003 *J. Phys.: Condens. Matter* **15** S2647
[32] Turrell G 1972 *Infrared and Raman Spectra of Crystals* (London: Academic) chapter 5
[33] Kampen T U, Salvan G, Paraian A, Himcinschi C, Kobitski A Yu, Friedrich M and Zahn D R T 2003 *Appl. Surf. Sci.* **212/213** 501
[34] Ferraro J R and Nakamoto K *Introductory Raman Spectroscopy* (London: Academic)
[35] Aroca R, Jennings C, Loutfy R O and Hor A M 1986 *J. Phys. C: Solid State Phys.* **90** 5255
[36] Woollam J A, Johs B, Herzinger C M, Hilfiker J N, Synowicki R and Bungay C 1999 *SPIE Proc.* **CR72**
[37] Johs B and Herzinger C 1995 *Guide to Using WVASE32* (Lincoln, NE: J A Woollam Co., Inc.)